



Mechanical properties of human dental enamel on the nanometre scale

S. Habelitz^a, S.J. Marshall^{a,*}, G.W. Marshall Jr^a, M. Balooch^b

^a Department of Preventive and Restorative Dental Sciences, University of California, 707 Parnassus Avenue, D2246 San Francisco, CA 94143-0758, USA

^b Department of Chemistry and Materials Science, Lawrence Livermore National Laboratory, Livermore, CA 94550, USA

Accepted 1 July 2000

Abstract

Atomic force microscopy (AFM) combined with a nano-indentation technique was used to reveal the structure and to perform site-specific mechanical testing of the enamel of third molars. Nano-indentations (size < 500 nm) were made in the cusp area to measure the mechanical properties of single enamel rods at different orientations. The influence of etching on the physical properties was studied and etching conditions that did not significantly alter the plastic–elastic response of enamel were defined. Elasticity and hardness were found to be a function of the microstructural texture. Mean Young's moduli of $87.5 (\pm 2.2)$ and $72.7 (\pm 4.5)$ GPa and mean hardness of 3.9 ± 0.3 and 3.3 ± 0.3 GPa were measured in directions parallel and perpendicular to the enamel rods, respectively. Analysis of variance showed that the differences were significant. The observed anisotropy of enamel is related to the alignment of fibre-like apatite crystals and the composite nature of enamel rods. Mechanical properties were also studied at different locations on single enamel rods. Compared to those in the head area of the rods, Young's moduli and hardness were lower in the tail area and in the inter-rod enamel, which can be attributed to changes in crystal orientation and the higher content of soft organic tissue in these areas. © 2001 Elsevier Science Ltd. All rights reserved.

Keywords: Enamel rod; Nanohardness; Modulus; Tooth orientation; Anisotropy; Etching

1. Introduction

Knowledge of the mechanical properties of microstructural features in dental enamel is important to calculating stress dissipation in the tooth, to developing biomimetic restorative materials and to the execution of clinical dental preparations (Spears, 1997). Enamel's unique microstructure consists of aligned prisms or rods, which run approximately perpendicular from the dentine–enamel-junction towards the tooth surface

(Meckel et al., 1965; Ten Cate, 1989; Warshawsky, 1989). The ideal structure of these rods, as depicted in Fig. 1, is keyhole-like with an average width of about 5 μm . Each rod consists of tightly packed carbonated hydroxyapatite crystals (Young, 1974), which are covered by a nanometre-thin layer of enamelin and oriented along the rod axis as shown in Fig. 1. The interfacial area between rods is termed inter-rod enamel; it is protein rich and mostly a result of the incoherence of combining crystals of different orientation in that area (Weber, 1975; Warshawsky, 1989).

The highly oriented microstructure of enamel results in anisotropy of its mechanical properties. Macroscopic methods, such as acoustic impedance, flexural and ten-

* Corresponding author. Tel.: +1-415-4765992; fax: +1-415-4760858.

E-mail address: sallym@itsa.ucsf.edu (S.J. Marshall).

sile testing, have been used to determine the elasticity, strength and toughness of dental tissues (Bowen and Rodriguez, 1962; Rasmussen et al., 1976; Rasmussen, 1984; El Mowafy and Watts, 1986; Lin and Douglas, 1994). In a critical-angle reflection technique with applied ultrasonic waves, the elastic response of bovine enamel was found to be anisotropic (Lees and Rollins, 1972); elastic moduli of 125 and 115 GPa were measured in occlusal and longitudinal directions, respectively. The behaviour of the tooth during fracture was studied intensively by Rasmussen et al. (1976) and Rasmussen, (1984) both enamel and dentine are reportedly fractured in a brittle manner but only enamel exhibits a highly anisotropic fracture mode. In agreement with observations and theory for composite materials (Rice, 1988; He and Hutchinson, 1989), cracks tend to follow weak interfaces. Hence, crack propagation occurs preferentially along the inter-rod spaces parallel to the rod axes.

Studies of the micromechanical properties of teeth usually involve microhardness tests made with Vickers or Knoop indenters (von der Fehr, 1967). However, earlier studies could not show the effects of the tooth orientation on hardness (Davidson et al., 1974). A recent study by Xu et al. (1998) combining Vickers indentation and scanning electron microscopy (SEM) demonstrated anisotropy of the mechanical properties of enamel. Among other properties, hardness and Young's modulus were higher when measured on occlusal rather than longitudinal sections; for an individual tooth, hardness of 3.7 and 3.1 GPa and moduli of 98 and 86 GPa were determined on occlusal and longitudinal surfaces, respectively.

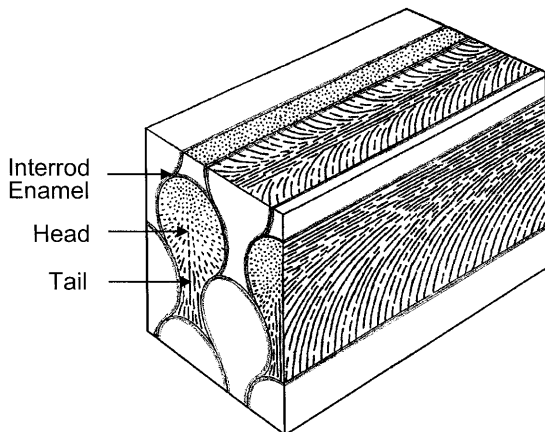


Fig. 1. Schematic drawing of enamel microstructure, showing keyhole-like rods of about 5 μm diameter aligned in parallel. Enamel rods are over 95% mineralised and contain aligned fibre-like apatite crystals with different orientations in the head and tail area. Inter-rod enamel is enriched in organic matter. Modified from Meckel et al. (1965).

Although such measurements on the macro- and micro-scale have taken into account the directional dependence of the properties, the methods do not permit measurement of the mechanical properties of single enamel rods. In order to study the isolated properties of enamel rods a method is required in which the indentation size is about one order of magnitude less than the area of interest, 5 μm . Nano-indenting is an excellent tool for this purpose. This depth-sensing technique allows measurement of Young's modulus and hardness in small features, even below 1 μm . Similar problems have been approached by several investigators who have applied nano-indentation techniques to biological tissues, e.g. the mechanical properties of peritubular and intertubular dentine (Kinney et al., 1996a,b) or of osteons and interstitial lamellae in trabecular and cortical bone (Rho et al., 1997; Zysset et al., 1999). Nano-indentation has also been applied to human enamel, but not in relation to rod orientation and surface preparation (Willems et al., 1993).

A further advantage of the atomic force-microscopy nano-indentation technique is the opportunity to use the nano-indenter of the same apparatus as a scanning probe. Thus, by means of piezo-elements, which can adjust for nanomovements of the tip in the z -direction, the topography of the sample is recorded and can be imaged. Hence, spatially resolved mapping of the mechanical properties and imaging with a resolution better than 500 nm are done with the same device.

For the present study, a modified atomic force microscope was used to make nano-indentations on longitudinal and occlusal sections of the enamel of four sound third molars. In order to study the anisotropic behaviour of single enamel rods, indentations were placed parallel and perpendicular to the rod axes. The study also reports on mechanical properties in relation to different areas of single rods, which are supposed to vary according to the orientation of crystals within them. The effect of etching on the mechanical properties was analysed by nano-indenting on enamel after different surface treatments.

2. Materials and methods

2.1. Specimen preparation

Human third molars were extracted from individuals as part of their dental treatment. Protocols were approved by the UCSF committee on human research and all individuals gave informed consent. The extracted teeth were sterilised by gamma irradiation (White et al., 1994) and stored (for less than 4 months) in deionized water at 4°C until prepared. Four teeth, three erupted and one impacted, were sectioned longitudinally. Part of the dentine was cut off occlusally about

5 mm below the dentine–enamel junction. Specimens were ground metallographically through a series of SiC abrasive papers down to 4000 mesh. They were then polished with water-based diamond suspensions (Buehler, Lake Bluff, IL) of 1.0 and 0.25 μm particle size, on soft polishing cloths. The buccal and lingual sides were ground with SiC paper (600 grit) to obtain a planoparallel disc. Samples were rinsed copiously under water after each polishing step. Finally, samples were cleaned ultrasonically in deionized water. Ultrasonication was limited to 30 s, as longer treatments may alter the plastic–elastic response of the surface area of enamel. Specimens were studied immediately after the final surface preparation. Longitudinally cut samples were first studied by nano-indentation. The same samples were then used to study the occlusal section. For this purpose, specimens were ground, polished and cleaned occlusally in the same manner as longitudinal sections. Initial atomic force-microscopic images frequently failed to reveal the enamel structure, so ‘selective etching’ was applied. Hydrochloric acid, HCl, and citric acid, $\text{C}_6\text{H}_8\text{O}_7$, were used. The influence of different concentrations and etching times on the nanoproperties was studied. As shown later, etching with 0.005 mol% citric acid for 5 s was found sufficient to reveal the microstructure. It was applied to all samples in which the enamel microstructure was not revealed directly after polishing. Occasionally, due to etching variability, it was necessary to repolish the specimen with 0.25 μm diamond paste to improve the surface quality. The mean roughness (R_a) was used as a measure of etching characteristics and was determined for areas of $20 \times 20 \mu\text{m}$ from the atomic force-microscopic images.

High-resolution images were obtained on dehydrated samples by scanning in the tapping mode using a silicon tip.

2.2. Nano-indentation

Specimens were studied in an atomic force microscope, Nanoscope III (Digital Instruments, Santa Barbara, CA), with the standard head replaced by a Triboscope indenter system (Hysitron Inc., Minneapolis, MN), as described elsewhere (Balooch et al., 1998). A sharp cube corner diamond indenter with a tip radius of about 20 nm was used for indentation and scanning imaging. Fused silica was used to calibrate the reduced elastic modulus and to define the tip area function for indentation depths between 50 and 600 nm. In order to find the right locations for indenting perpendicular or parallel to the axes of the enamel rods, the microstructure of the sample was studied first. Once a region exhibiting a parallel alignment of rods or a keyhole-like structure was observed, indentations were placed along lines, with a spacing of about 3 μm between indentations. An area of about $20 \times 20 \mu\text{m}$ was

examined for each spot selected. A load of 1500 μN was applied, resulting in indentation depths of around 300 nm. In a typical experiment, an indentation was made using a trapezoidal force profile by driving the indenter at a constant loading rate of 500 $\mu\text{N/s}$ into the material and holding it at this load for 3 s. The indenter was then withdrawn from the surface at a constant rate of 500 $\mu\text{N/s}$. A minimum of 100 indentations was made on occlusal and longitudinal sections of each tooth. Samples were maintained in the hydrated state during all the preparations and were examined immediately after the final polish. The indentations were made in a dry room atmosphere. Each series of indentations was finished within 60 min. Teeth were rehydrated in deionized water between series. Only the cusp area of the enamel was examined. Indentations made parallel to the enamel rod axis were classified by their locations: head area, tail area or inter-rod enamel. Mean Young’s modulus and hardness were calculated from at least ten indentations in these particular areas.

The indentation load–displacement data were analysed to determine the hardness, H , and the Young’s modulus, E , according to the method of Oliver and Pharr (1992). Power-law curves were fitted to the first 45% of the final unloading, and contact stiffness and contact depth were obtained by differentiating and extrapolating these curves. The Young’s modulus was calculated from the following equation:

$$\frac{1}{E_r} = \frac{(1 - \nu_s^2)}{E_s} + \frac{(1 - \nu_i^2)}{E_i} \quad (1)$$

where E_r is the reduced modulus; E_s the Young’s modulus of the specimen; E_i Young’s modulus of the indenter; ν_s and ν_i , the Poisson’s ratio of specimen and indenter, respectively. For a diamond indenter, E_i , 1141 GPa and ν_i , 0.07. According to the literature, an isotropic Poisson ratio for enamel of 0.28 was assumed (Waters, 1980) and was used for the calculations. Using possible variations of the Poisson’s ratio in the range of 0.2–0.3 affected the resulting Young’s modulus by less than 10%.

Hardness is defined as the maximum load, P_{max} , divided by the projected area of the contact impression, A , i.e.

$$H = \frac{P_{\text{max}}}{A} \quad (2)$$

ANOVA was applied to test for significant differences in hardness and Young’s modulus in relation to tooth orientation and tooth-to-tooth variations; $P < 0.05$ was considered significant. The degree of anisotropy, degA , was determined according to:

$$\text{deg A} = \left(\frac{M_{\text{parallel}}}{M_{\text{perpendicular}}} \right) 100\% - 100 \quad (3)$$

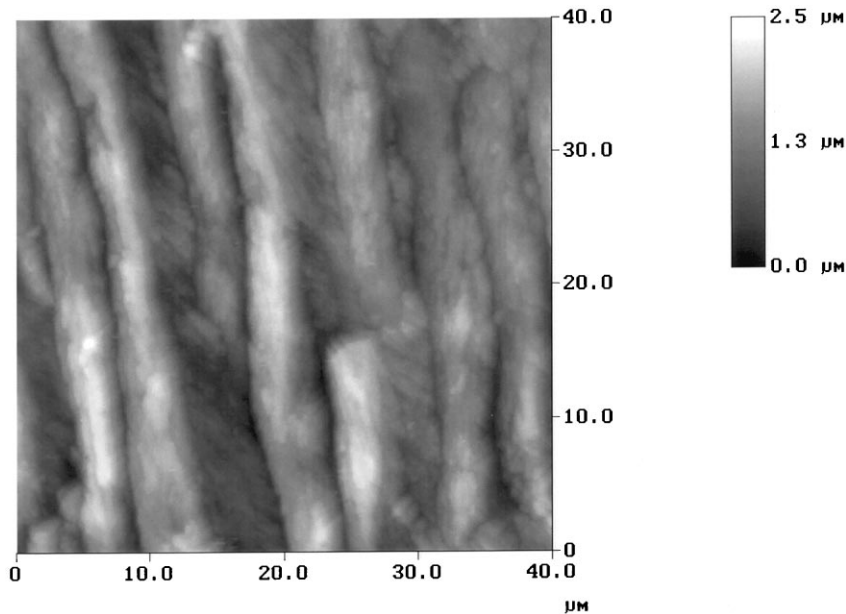


Fig. 2. Atomic force-microscopic image of enamel rods obtained on a longitudinal section; specimen etched with 0.05 mol.% HCl for 20 s.

with M , the mean value calculated (Habelitz et al., 1997).

3. Results

In order to reveal the microstructure of enamel, acid etching is usually applied (Marshall et al., 1975; Silverstone et al., 1975). However, nano-indentations only involve a thin surface layer, so the effect of surface preparation on the mechanical properties must be taken into account if samples are etched chemically. Surface treatments have to be found that allow, on the one hand, observation of the enamel microstructure and, on the other, minimise any alterations of the mechanical properties of the surface layer to be studied by nano-indentation. Polished and ultrasonically cleaned specimens only occasionally showed enough difference in height between the organic and inorganic matrix to reveal the rod-like architecture of enamel. Therefore, selective etching was applied. Fig. 2 shows an image obtained from a longitudinal section after etching in 0.05 mol.% HCl for 20 s: the highly textured microstructure of enamel is revealed; rods of about 5 μm diameter are aligned in parallel, but are not straight and in some cases appear interwoven, as also observed by others (Sturdevant et al., 1995; Xu et al., 1998). Fig. 3 is an image of an occlusal section of enamel etched with 0.1 mol.% citric acid for 10 s. The inorganic crystalline compound was dissolved preferentially and hence the organic matrix appears pronounced in this topographi-

cal view; the characteristic rod-like structure, partially keyhole-like in appearance, of an occlusal section through enamel is seen.

To study the effect of etching on the mechanical properties, nano-indentations were made on enamel after different surface treatments. Fig. 4 shows the load–displacement curves obtained by indenting on polished enamel sections with unetched, citric acid- and hydrochloric acid-etched surfaces. In comparison with the unetched samples, indentation depth increased dramatically after etching, resulting in lower hardness. Whereas the unetched sample had a nanohardness of around 3.3 GPa, hardness of below 2 GPa was usually obtained if samples had been etched. The elastic modulus, obtained from the slope of the unloading curve, was also altered in the etched samples. The modulus dropped from around 80 GPa for the unetched sample to around 55 GPa after etching with 0.1 mol.% citric acid. When a 0.05 mol.% solution of HCl had been applied, a relatively unstable unloading curve was recorded, causing high variations in the modulus of between 30 and 200 GPa.

Etching also influenced the surface roughness of the sample, which has a further influence on nanohardness and elasticity (Bobji and Biswas, 1998). Whereas a mean roughness (R_a) of below 3 nm was measured after polishing and ultrasonication, R_a increased to 200 and 400 nm after etching with 0.1 mol.% citric acid or 0.05 mol.% HCl, respectively. Because of the effect on the mechanical properties, the etching conditions were modified. Etching with 0.005 mol.% citric acid for 5 sec

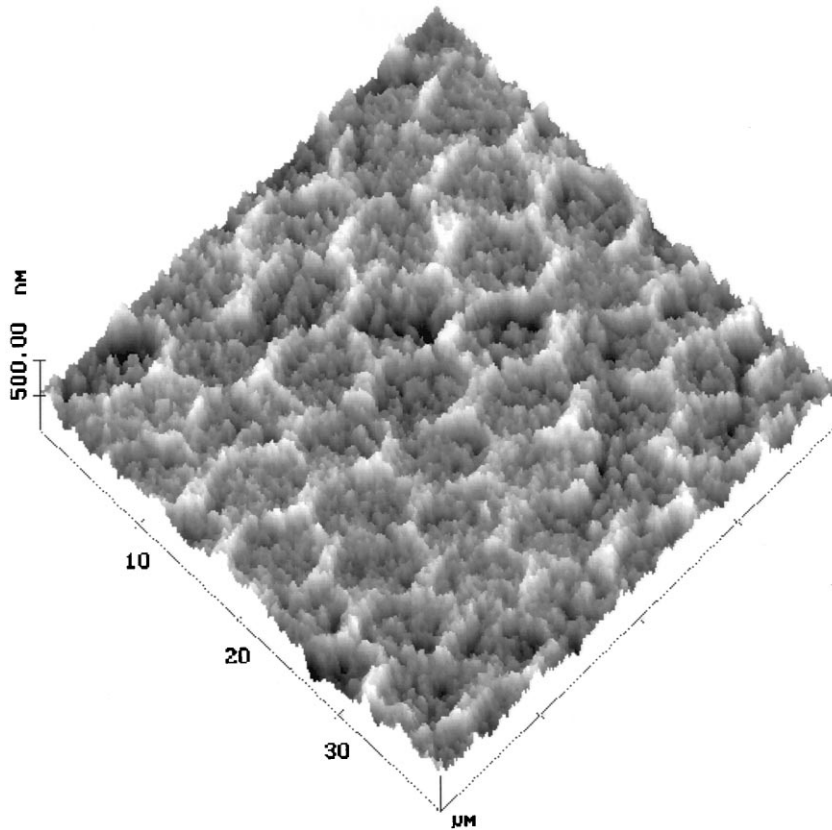


Fig. 3. Atomic force-microscopic image of enamel rods obtained on an occlusal section; specimen etched with 0.1 mol% citric acid for 10 s.

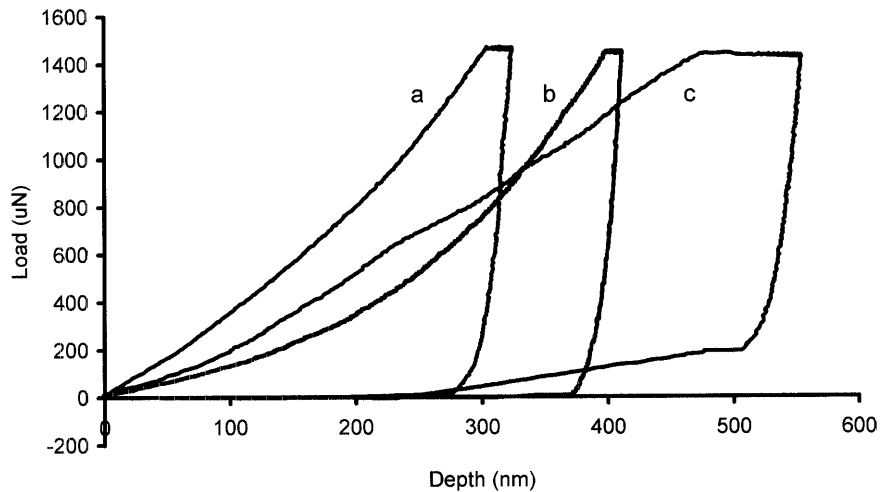


Fig. 4. Load-displacement curves obtained by nano-indentation on polished enamel (a) unetched, (b) etched with 0.1 mol% citric acid for 10 s and (c) etched with 0.05 mol% HCl for 20 s.

was sufficient to reveal the enamel microstructure and did not cause significant differences in the modulus and hardness compared to those of unetched samples in the

same area of the enamel. Hence, it can be assumed that this etching did not alter the mechanical properties significantly.

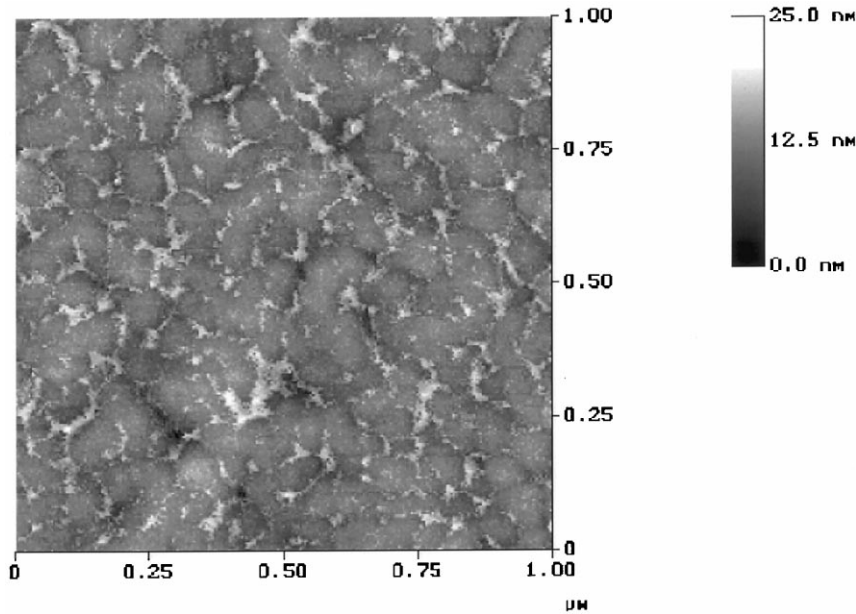


Fig. 5. Atomic force-microscopic image of head area of a single enamel rod on an occlusal section. Single apatite crystals of about 50 nm diameter covered with a nanometre thin cuticle of proteins are observed. Specimen etched with 0.005 mol% citric acid for 5 s image obtained in tapping mode.

Surface roughness was used as a measure of adequate etching. Accurate evaluation of elasticity and hardness was ensured at a mean surface roughness R_a of below 10 nm (usually about 5 nm was obtained). Fig. 5 shows an image obtained in tapping mode on the occlusal section of enamel etched for 5 s with 0.005 mol% citric acid. At this high resolution, single apatite crystals of about 50 nm width, separated by a thin cuticle of enamelin, are seen. The high surface quality of the sample even after etching is demonstrated.

The same etchant revealed similar surface qualities on longitudinal sections of enamel as on occlusal sections. Fig. 6 and Fig. 7 show images of nano-indentations on an occlusal section of enamel. The keyhole-like structure is seen, ensuring that enamel rods were sectioned perpendicular to their axes. Hence, indentations were made parallel to the rod axis. The inverted image in Fig. 7, reveals, at a higher magnification, the surface roughness of a single rod and shows that it is much less than the indentation depth of about 300 nm.

The image in Fig. 8 shows nano-indentations on a longitudinal section of enamel. Here, rods were cut parallel to their axis. The aligned microstructure of rods is seen. Indentations were made perpendicular to the rod axis.

From each indentation, site-specific values for the elastic modulus and the hardness were obtained. Table 1 shows the overall results obtained on three erupted and one impacted third molars in relation to the direc-

tion of indentation. All specimens exhibited higher Young's moduli and hardness if indentations were made parallel to the rod axis. The Young's modulus varied in the range between 85 and 90 GPa; hardness was between 3.4 and 3.9 GPa. When the indentations were placed perpendicular to the rod axis, the elastic modulus and hardness decreased to between 70 and 77 GPa and 3.0–3.5 GPa, respectively. The values obtained parallel and perpendicular to the rod axis were significantly different at 95% confidence ($P < 0.05$), as tested by single-factor ANOVA. The degrees of anisotropy varied between 5 and 30%. Average values over all samples also are presented in Table 1.

As shown in Fig. 6, nano-indentations were placed along lines on the specimens and thus appear at different locations on the enamel rods. To compare the influence of indenting at different locations within a rod, indentations from the head and tail area and from the inter-rod enamel were grouped and compared. Average values of the mechanical properties obtained from these indentations are shown in Tables 2 and 3. Compared with the values obtained from the head area of the rods, Young's moduli and hardness tended to be lower in both the tail area and the inter-rod enamel. However, the lower moduli in the tail area and inter-rod enamel were not significantly different from those obtained in the head area. Significant differences ($P < 0.05$) in mechanical properties at different locations on the enamel were only observed for hardness.

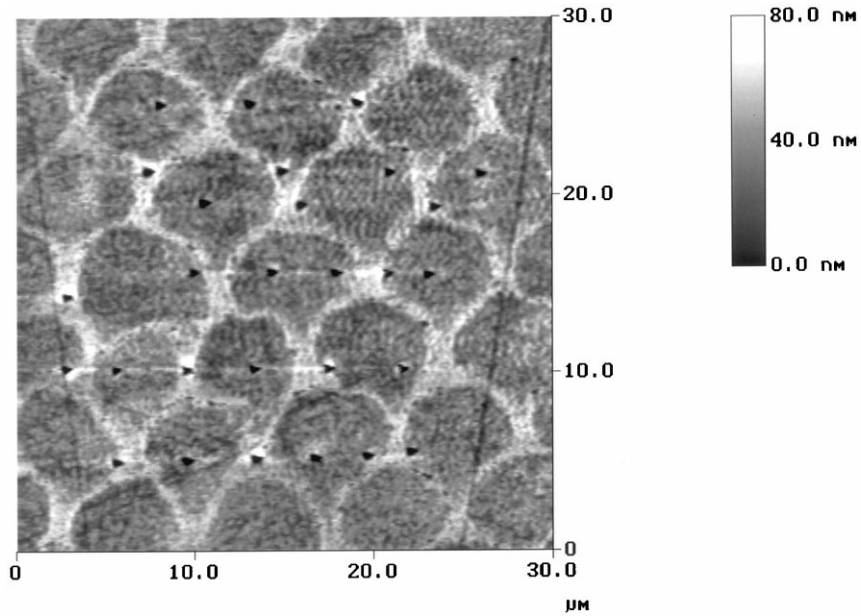


Fig. 6. Image of nano-indentations on an occlusal enamel section obtained with modified atomic force microscopy. Due to the keyhole-like appearance of the enamel microstructure, indenter axis and enamel rod axes are aligned in parallel.

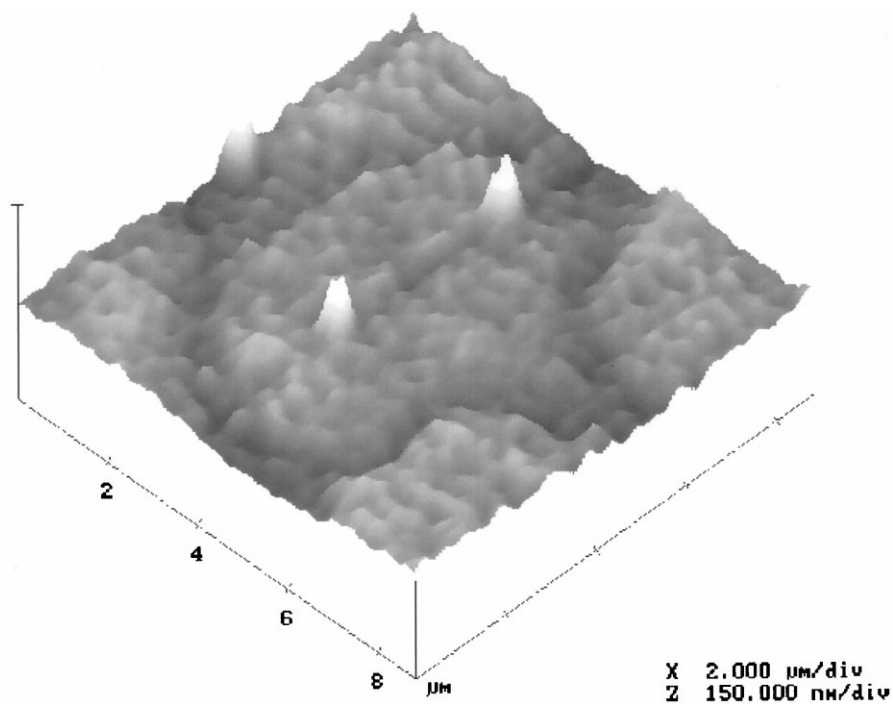


Fig. 7. Inverted image of nano-indentations on an occlusal enamel section obtained with modified atomic force microscope, showing that indentation depth is much larger than surface roughness.

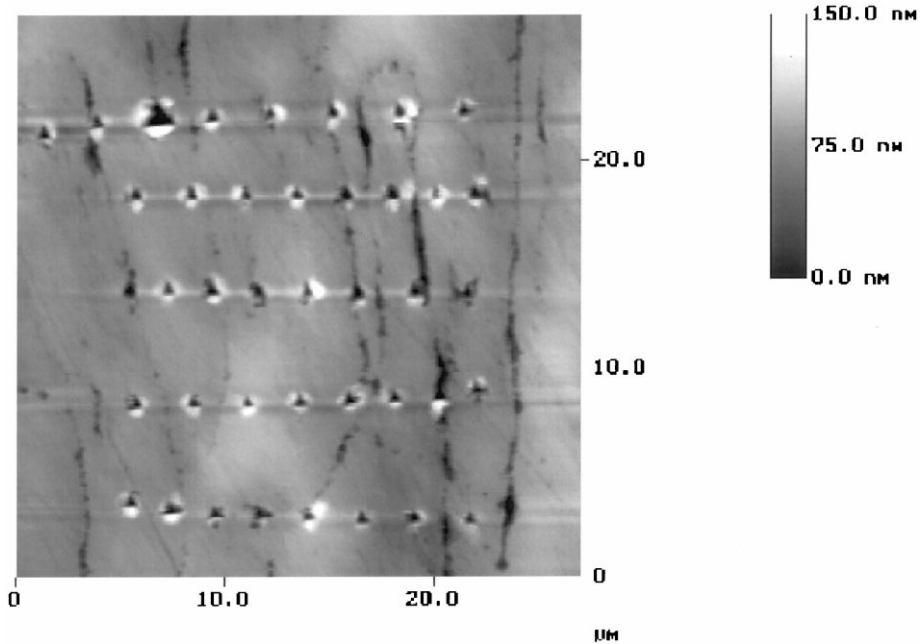


Fig. 8. Image of nano-indentations on a longitudinal section of enamel obtained with modified atomic force microscope. A parallel arrangement of enamel rods is observed. Indenter axis is aligned perpendicular to enamel rod axes.

Table 1
Anisotropy of enamel

	Tooth number				Overall
	1 erupted	2 erupted	3 erupted	4 impacted	
<i>E</i> -modulus (GPa) parallel	89.6 ± 5.9	87.2 ± 8.5	84.6 ± 14.8	88.6 ± 9.4	87.5 ± 2.1
<i>E</i> -modulus (GPa) perpendicular	68.5 ± 4.0	78.3 ± 3.6	74.1 ± 7.7	69.6 ± 4.2	72.7 ± 4.4
<i>P</i> -value	10 ⁻⁷⁵	10 ⁻³⁵	10 ⁻¹⁴	10 ⁻¹⁵	10 ⁻¹⁸
DegA (%)	30	11	14	27	20
Nanohardness (GPa) parallel	3.4 ± 0.40	4.1 ± 0.32	3.8 ± 0.33	4.0 ± 0.38	3.8 ± 0.31
Nanohardness (GPa) perpendicular	2.9 ± 0.40	3.6 ± 0.24	3.6 ± 0.31	3.1 ± 0.42	3.3 ± 0.35
<i>P</i> -value	10 ⁻¹⁷	10 ⁻⁸	10 ⁻⁴	10 ⁻⁷	10 ⁻⁸
DegA (%)	18	15	5	28	16

Table 2
Mechanical properties of the head and tail area of enamel rods

	Tooth Number	Tooth Number			Overall
		Location	2	3	
Young's modulus (GPa)	Head area	90.7 ± 7.6	84.6 ± 13.8	91.6 ± 5.7	88.0 ± 8.6
	Tail area	79.3 ± 7.9	80.3 ± 15.5	87.5 ± 2.9	80.3 ± 7.2
<i>P</i> -value		0.09	0.2	0.09	0.004
Hardness (GPa)	Head area	4.3 ± 0.3	4.1 ± 0.3	3.9 ± 0.2	4.3 ± 0.4
	Tail area	3.9 ± 0.5	3.6 ± 0.3	3.8 ± 0.1	3.7 ± 0.4
<i>P</i> -value		0.002	10 ⁻³	0.5	10 ⁻⁸

Table 3

Mechanical properties of the head area of enamel rods and the inter-rod enamel

	Tooth number				Overall
	Location	2	3	4	
<i>E</i> -modulus (GPa)	Head area	90.7 ± 7.6	84.6 ± 8.6	91.5 ± 5.9	88.0 ± 8.6
	Inter-rod enamel	89.9 ± 4.9	80.3 ± 15.5	87.8 ± 2.9	86.4 ± 11.7
<i>P</i> -value		0.68	0.4	0.06	0.4
Hardness (GPa)	Head area	4.3 ± 0.3	4.1 ± 0.3	3.9 ± 0.2	4.3 ± 0.4
	Inter-rod	4.1 ± 0.1	3.6 ± 0.3	3.6 ± 0.3	3.9 ± 0.4
<i>P</i> -value		0.002	10 ⁻⁶	0.004	10 ⁻⁵

4. Discussion

The combination of atomic force microscopy and nano-indentation allows both observation of enamel microstructure and measurement of the mechanical properties of enamel microfeatures. However, in order to reveal the microstructure acid etching is usually required, which affects the elastic–plastic response of the enamel to nano-indentation. Therefore, etching conditions had to be established that provided sufficient definition of the rod-like structure, but did not alter significantly the mechanical properties.

The ‘rule of thumb’ that a roughness (R_a) of less than 10% of the indentation depth will not affect the measurement of elastic modulus and hardness is not necessarily true for etched materials. Etching of highly polished enamel not only increases the surface roughness but also changes the chemical composition within the etched layer. In order to minimise any effect of etching on the mechanical properties of enamel, the acid attack has to be minimal. Therefore, we used a highly dilute etchant and a short etching time. From a series of different etching procedures, etching with 0.005 mol% citric acid for 5 s was found to be suitable for this purpose. It resulted in a low surface roughness (R_a), usually below 5 nm, as compared with the depth of nano-indentation, which exceeded 300 nm.

Nano-indentations were made on specimens etched according to this protocol. As shown in Table 1, highly significant differences in Young’s modulus and hardness were found if indentations were performed parallel or perpendicular to the enamel rod axis. Modulus and hardness were higher if indenter axis and rod axis were parallel, giving rise to anisotropy of up to 30%. The Young’s moduli of the four individual teeth studied are in the range of 85–90 and 70–77 GPa in directions parallel and perpendicular to the rod axis, respectively. They are thus of the same order as moduli reported by Xu et al. (1998). The dependence of the mechanical properties on the orientation of the tooth originates in the texture of fibre-like apatite crystals in the enamel rods. These fibres are mostly single crystalline and point

in the head area with their *c*-axes parallel to the rod axes, as shown in Fig. 1. Single hydroxyapatite and fluoroapatite crystals reportedly show elastic anisotropy (Katz and Ukraincik, 1971; Sha et al., 1994): Young’s moduli of around 145 and 125 GPa¹ have been measured parallel and perpendicular to the *c*-axis of the hexagonal apatite crystals, respectively. Thus, the observed anisotropy of enamel with a higher elastic modulus parallel to the rod than perpendicular to it, is predominantly a result of the crystal anisotropy and texture.

We have found no reference to anisotropy of the hardness of single apatite crystals. However, in crystalline materials, higher elastic moduli are usually related to higher hardness (Waters, 1980). Therefore, it is assumed that the origin of the anisotropy of hardness of enamel also is mostly a result of the anisotropy and alignment of apatite crystals. The nanohardness values agree with the microhardness values found by Xu et al. (1998). Biovariability in human enamel and the differences in the techniques used, e.g. indenter size and shape, are factors that might explain small differences.

Compared to those for pure single hydroxy- or fluoroapatite crystals, we found significantly lower elastic moduli for enamel. We attribute this difference to the fact that apatite crystals in enamel are highly defective and contain at least 2 wt.% carbonate ions (Teraoka et al., 1998) and that enamel is composed of at least 5 vol.% of organic tissues and water, both of which cause a decrease in the elastic modulus.

An additional contribution to the anisotropic behaviour of enamel rods is attributable to their composite nature. As pointed out by Katz (1971) and Spears (1997), stresses will be carried by the high-stiffness crystals if indentations are made parallel to the rod axis, when higher elastic moduli and hardness will be obtained. In contrast, when stress is applied across the crystals, it is carried by the low stiffness, deformable organic matrix surrounding them, producing lower elastic moduli and hardness in this direction. As a conse-

¹ Corresponds to [1210] axis.

quence, the resulting anisotropy of enamel can increase to above that of the anisotropy of single apatite crystals.

The ideal apatite crystal arrangement in enamel rods is shown in Fig. 1. In the head area the fibre-like crystals are aligned parallel to the rod axes. Towards the tail area, they flare laterally, attaining an almost perpendicular orientation at the inter-rod enamel. In Table 2, the mechanical properties of the head and tail area are juxtaposed. Young's modulus and hardness were lower in the tail area in all teeth studied, which we attribute to the change in crystal orientation in this area. However, the differences for the Young's modulus were not statistically significant.

The mechanical properties of the head area of the enamel rods and of the inter-rod enamel are compared in Table 3. Young's moduli and hardness are lower in the inter-rod enamel, which we attribute mostly to the higher content of elastic and soft organic tissue in this area. However, the Young's moduli values were not significantly different ($P > 0.05$), which might be due to the fact that the inter-rod space shows high variability of mineral content and is so small that indentations did not hit exclusively the organic soft tissue.

However, nanohardness was significantly lower in the inter-rod enamel. Besides the higher content of proteins in this area, the effect of selective etching contributes to the lower hardness obtained. As shown in the topographic profiles of the images in Figs. 3, 6 and 7, citric acid preferentially dissolves the crystalline phase and thus the protein-rich inter-rod space may become more prominent. The etching depth was usually between 20 and 50 nm. Hence, indentations placed on the inter-rod enamel increase in depth not only because of the naturally higher protein content in this area but also because etching alters the composition in this area, e.g. the dissolution of the crystalline phase. This observation shows the importance of adequate surface preparation when nano-indentations are applied.

5. Conclusions

Atomic force microscopy-based nano-indenting is an excellent tool for measuring the site-specific mechanical properties of enamel rods. However, as the indentation size and depth are very small (around 300 nm), particular care has to be taken with surface preparation. Therefore, in a preliminary study, etching conditions were established that permitted visualization of the enamel microstructure and also ensured the accuracy of the measurement of the elastic modulus and hardness. Our study of the dependence of the mechanical properties of enamel rods on their orientation showed that higher moduli and hardness occur parallel to the rod axes. Mean Young's moduli of $87.5 (\pm 2.2)$ and 72.7

(± 4.5) GPa and mean hardness of $3.9 (\pm 0.3)$ and $3.8 (\pm 0.4)$ GPa were found in directions parallel and perpendicular to the enamel rods, respectively. The observed anisotropy of up to 30% is attributed to the anisotropy and alignment of fibre-like apatite crystals within the rods and to the composite architecture of enamel. Elastic modulus and hardness are lower in the inter-rod enamel, which is attributed to the higher content of organic soft tissue. Due to changes in the crystal orientation in the tail area, Young's modulus and hardness are lower in this area.

Acknowledgements

This research was supported by NIH/NIDCR Grant RO1-DE 13029.

References

- Balooch, M., Wu-Magidi, I.C., Lundkvist, A.S., Balazs, A., Marshall, S.J., Marshall, G.W., Seikhaus, W.J., Kinney, J.H., 1998. Viscoelastic properties of demineralized human dentin in water with atomic force microscopy (AFM)-based indentation. *J. Biomed. Mater. Res.* 40, 539–544.
- Bowen, R.L., Rodriguez, M.S., 1962. Tensile strength and modulus of elasticity of tooth structure and several restorative materials. *J. Am. Dent. Assoc.* 64, 378–387.
- Bobji, M.S., Biswas, S.K., 1998. Estimation of hardness by nanoindentation of rough surfaces. *J. Mater. Res.* 13, 3227–3233.
- Davidson, C.L., Hoekstra, I.S., Arends, J., 1974. Microhardness of sound decalcified and etched tooth enamel related to Ca content. *Caries Res.* 8, 135–144.
- El Mowafy, O.M., Watts, D.C., 1986. Fracture toughness of human dentin. *J. Dent. Res.* 65, 677–681.
- Habelitz, S., Carl, G., Ruessel, C., Thiel, S., Gerth, U., Schnapp, J.D., Jordanov, A., Knake, H., 1997. Mechanical properties of oriented mica glass ceramic. *J. Non-Crystalline Solids.* 220, 291–298.
- He, M.Y., Hutchinson, J.W., 1989. Crack deflection at an interface between dissimilar elastic materials. *Int. J. Solids Struct.* 25, 1053–1067.
- Katz, J.L., Ukrainik, K., 1971. On the anisotropic elastic properties of hydroxyapatite. *J. Biomech.* 4, 221–227.
- Kinney, J.H., Balooch, M., Marshall, S.J., Marshall, G.W., Weihs, T.P., 1996a. Hardness and Young's modulus of human peritubular and intertubular dentine. *Arch. Oral Biol.* 41, 9–13.
- Kinney, J.H., Balooch, M., Marshall, S.J., Marshall, G.W., Weihs, T.P., 1996b. Atomic force microscope measurements of the hardness and elasticity of peritubular and intertubular dentin. *J. Biomech. Eng.* 118, 133–135.
- Lees, S., Rollins, F.R., 1972. Anisotropy of hard dental tissues. *J. Biomech.* 5, 557–566.
- Lin, C.P., Douglas, W.H., 1994. Structure-property relations and crack resistance at the bovine dentin-enamel junction. *J. Dent. Res.* 73, 1072–1078.

- Marshall, G.W., Olson, L.M., Lee, C.V., 1975. SEM investigation of the variability of enamel surfaces after simulated clinical acid etching for pit and fissure sealants. *J. Dent. Res.* 54, 1222–1231.
- Meckel, A.H., Griebstein, W.J., Neal, R.J., 1965. Structure of mature human dental enamel as observed by electron microscopy. *Arch. Oral. Biol.* 10, 775–783.
- Oliver, W.C., Pharr, G.M., 1992. An improved technique for determining hardness and elastic modulus using load and displacement sensing indentation experiments. *J. Mater. Res.* 7, 1564–1583.
- Rasmussen, S.T., 1984. Fracture properties of human teeth in proximity to the dentinoenamel junction. *J. Dent. Res.* 63, 1279–1283.
- Rasmussen, S.T., Patchin, R.E., Scott, D.B., Heuer, A.H., 1976. Fracture properties of human enamel and dentin. *J. Dent. Res.* 55, 154–164.
- Rice, J.R., 1988. Elastic fracture mechanics concepts for interfacial cracks. *J. Appl. Mech.* 55, 98–103.
- Rho, J.Y., Tsui, T.Y., Pharr, G.M., 1997. Elastic properties of human cortical and trabecular lamellar bone measured by nanoindentation. *Biomaterials* 18, 1325–1330.
- Silverstone, L.M., Saxton, C.A., Dogon, I.L., Fejerskov, O., 1975. Variation in the pattern of acid etching of human dental enamel examined by scanning electron microscopy. *Caries. Res.* 9, 373–387.
- Sha, M.C., Li, Z., Bradt, R.C., 1994. Single-crystal elastic constants of fluorapatite. *J. Appl. Phys.* 75, 7784–7787.
- Spears, I.R., 1997. A three dimensional finite element model of prismatic enamel: a reappraisal of the data of the Young's modulus of enamel. *J. Dent. Res.* 76, 1690–1697.
- Sturdevant CM, Robertson TM, Heymann HO, Sturdevant JR 1995. Operative Dentsitry, third ed. St. Louis, MO: Mosby chapters 2 and 7.
- Ten Cate, A.R., 1989. Oral Histology: Development, Structure, and Function, third ed. Mosby, St. Louis, MO.
- Teraoka, K., Ito, A., Maekawa, K., Onuma, K., Tateishi, T., Tsutsumi, S., 1998. Mechanical properties of hydroxyapatite and OH-carbonated hydroxyapatite single crystals. *J. Dent. Res.* 77, 1560–1568.
- Warshawsky, H., 1989. Organization of crystals in enamel. *Anat. Rec.* 224, 242–262.
- Waters, N.E., 1980. Some mechanical and physical properties of teeth. In: Vincent, J.F.V., Currey, J.D. (Eds.), *The Mechanical Properties of Biological Materials*. Cambridge University Press, Cambridge, pp. 99–136.
- Willems, G., Celis, J.P., Lambrechts, P., Braem, M., Vanherle, G., 1993. Hardness and Young's modulus determined by nanoindentation technique of filler particles of dental restorative materials compared with human enamel. *J. Biomed. Mater. Res.* 27, 747–755.
- Weber, D.F., 1975. Sheath configurations in human cuspal enamel. *J. Morphol.* 141, 479–487.
- White, J.M., Goodis, H.E., Marshall, S.J., Marshall, G.W., 1994. Sterilization of teeth by gamma radiation. *J. Dent. Res.* 73, 1560–1567.
- von der Fehr, F.R., 1967. A study of carious lesions produced in vivo in unabraded, abraded, exposed, and F-treated human enamel surfaces, with emphasis on the X-ray dense outer layer. *Arch. Oral. Biol.* 12, 797–814.
- Xu, H.H.K., Smith, D.T., Jahanmir, S., Romberg, E., Kelly, J.R., Thompson, V.P., Rekow, E.D., 1998. Indentation damage and mechanical properties of human enamel and dentin. *J. Dent. Res.* 77, 472–480.
- Young, R.A., 1974. Implications of atomic substitutions and other structural details in apatites. *J. Dent. Res. Suppl.* 53 (2), 193–203.
- Zysset, P.K., Guo, X.E., Hoffer, C.E., Moore, K.E., Goldstein, S.A., 1999. Elastic modulus and hardness of cortical and trabecular bone lamellae measured by nanoindentation in the human femur. *J. Biomech.* 32, 1005–1012.